Cancer Research

Threshold Analysis and Biodistribution of Fluorescently Labeled Bevacizumab in Human Breast Cancer

Maximilian Koch[1,2], Johannes S. de Jong[3], Jürgen Glatz[1,2], Panagiotis Symvoulidis[1,2], Laetitia E. Lamberts[4], Arthur L.L. Adams[5], Mariëtte E.G. Kranendonk[3], Anton G.T. Terwisscha van Scheltinga[4,6], Michaela Aichler[7], Liesbeth Jansen[8], Jakob de Vries[8], Marjolijn N. Lub-de Hooge[6], Carolien P. Schröder[4], Annelies Jorritsma-Smit[6], Matthijs D. Linssen[6], Esther de Boer[8], Bert van der Vegt[9], Wouter B. Nagengast[10], Sjoerd G. Elias[11], Sabrina Oliveira[12], Arjen J. Witkamp[13], Willem P.T.M. Mali[5], Elsken Van der Wall[14], P. Beatriz Garcia-Allende[1,2], Paul J. van Diest[3], Elisabeth G.E. de Vries[4], Axel Walch[7], Gooitzen M. van Dam[8,15], and Vasilis Ntziachristos[1,2]

Abstract

In vivo tumor labeling with fluorescent agents may assist endoscopic and surgical guidance for cancer therapy as well as create opportunities to directly observe cancer biology in patients. However, malignant and nonmalignant tissues are usually distinguished on fluorescence images by applying empirically determined fluorescence intensity thresholds. Here, we report the development of fSTREAM, a set of analytic methods designed to streamline the analysis of surgically excised breast tissues by collecting and statistically processing hybrid multiscale fluorescence, color, and histology readouts toward precision fluorescence imaging. fSTREAM addresses core questions of how to relate fluorescence intensity to tumor tissue and how to quantitatively assign a normalized threshold that sufficiently differentiates tumor tissue from healthy tissue. Using fSTREAM we assessed human breast tumors stained *in vivo* with fluorescent bevacizumab at microdose levels. Showing that detection of such levels is achievable, we validated fSTREAM for high-resolution mapping of the spatial pattern of labeled antibody and its relation to the underlying cancer pathophysiology and tumor border on a per patient basis. We demonstrated a 98% sensitivity and 79% specificity when using labeled bevacizumab to outline the tumor mass. Overall, our results illustrate a quantitative approach to relate fluorescence signals to malignant tissues and improve the theranostic application of fluorescence molecular imaging. *Cancer Res; 77(3); 623–31. ©2016 AACR.*

[1]Chair for Biological Imaging, Technical University of Munich, München, Germany. [2]Institute for Biological and Medical Imaging, Helmholtz Zentrum München, München, Germany. [3]Department of Pathology, University Medical Center Utrecht, Utrecht, the Netherlands. [4]Department of Medical Oncology, University of Groningen, University Medical Center Groningen, Groningen, the Netherlands. [5]Department of Radiology, University Medical Center Utrecht, Utrecht, the Netherlands. [6]Hospital and Clinical Pharmacy, University of Groningen, University Medical Center Groningen, the Netherlands. [7]Research Unit Analytical Pathology, Helmholtz Zentrum München, München, Germany. [8]Department of Surgery, University of Groningen, University Medical Center Groningen, the Netherlands. [9]Department of Pathology, University of Groningen, University Medical Center Groningen, the Netherlands. [10]Department of Gastroenterology, University of Groningen, University Medical Center Groningen, Groningen, the Netherlands. [11]Julius Center for Health Sciences and Primary Care, Cell Biology, University Medical Center Utrecht, Utrecht, the Netherlands. [12]Department of Biology, University Medical Center Utrecht, Utrecht, the Netherlands. [13]Department of Surgery, University Medical Center Utrecht, Utrecht, the Netherlands. [14]Department of Medical Oncology, Utrecht University, University Medical Center Utrecht, Utrecht, the Netherlands. [15]Department of Nuclear Medicine and Molecular Imaging and Intensive Care, University of Groningen, University Medical Center Groningen, Groningen, the Netherlands.

Note: Supplementary data for this article are available at Cancer Research Online (http://cancerres.aacrjournals.org/).

Corresponding Author: Vasilis Ntziachristos, Helmholtz Zentrum München, Ingolstädter Landstrasse 1, Neuherberg D-85764, Germany. Phone: 49-089-3187-3852; Fax: 49-089-3187-3008; E-mail: v.ntziachristos@tum.de

doi: 10.1158/0008-5472.CAN-16-1773

Introduction

Clinical translation of fluorescence agents that target cancer has the potential to guide surgical and endoscopy procedures, improving upon the limitations of human vision (1, 2). Several studies have received regulatory approvals to administer non–FDA-approved targeted fluorescent agents to humans (see ClinicalTrials.gov NCT01508572, NCT02113202, NCT01972373, NCT02129933, NCT01987375, NCT02415881). Applied topically or systemically, targeted fluorescence agents are expected to change the landscape of interventional guidance by steering biopsy, improving disease detection and driving accurate theranostics (3). Several studies have recently demonstrated the potential of using targeted fluorescent reporters to guide human surgery and endoscopy (3–7).

In addition to intraoperative guidance, *in vivo* cancer staining in patients scheduled for surgery or endoscopy may offer new insights in tumor physiology and agent biodistribution. Contrary to tissue histopathology that uses *ex vivo* staining, histologic analysis of human specimen stained *in vivo* can reveal functional characteristics of the tumor and its microenvironment associated with agent delivery, biodistribution and targeting, on a per-patient basis and at resolutions not available to macroscopic optical imaging or radiologic imaging.

However, an important and so far unsolved problem in *in vivo* fluorescence cancer imaging is the uncertain relation of

Table 1. Global sensitivity and specificity values

Sensitivity	Specificity	Threshold of S (presence of maximum normalized fluorescence value)
0.9000	0.9274	13.2%
0.9500	0.8775	9.8%
0.9800	0.7882	6.5%

fluorescence intensity to the underlying tumor extent. Fluorescence images obtained *in vivo* are diffusive (low resolution) in nature and do not delineate tumors with precision. Consequently, it becomes challenging to set an unbiased fluorescence threshold that will allow explicit differentiation of malignant from healthy tissue. As fluorescence molecular imaging is increasingly considered for clinical application, it becomes critical to develop methods that lead to accurate tissue classification and reveal the relation between administered agent and tumor extent.

In this work, we developed an analytic method that sought to deliver, objective criteria for fluorescence-based disease detection and differentiation from nondiseased tissues, toward precision fluorescence imaging. The study was based on clinical molecular imaging of breast cancer using fluorescence-labeled bevacizumab and had three objectives. First, it sought to establish the spatial relationship between the distribution of the antibody and the underlying tumor spatial extent, as it relates to the intraoperative identification of human breast cancer and cancer margins and quantitatively identify a fluorescence threshold for distinguishing malignant from nonmalignant tissue. Of particular interest herein was the development of a fluorescence threshold that is normalized and is not affected by variations of the amount of agent administered or agent dilution variations in each patient. Second, it inquired, in high-resolution, the spatial-pattern of labeled antibody within human cancer, a parameter not previously resolved by radiologic methods and generally unknown due to the effects of interstitial pressure gradients and abnormal tumor vascularization. Finally, the study identified the sensitivity and specificity of cancer detection using bevacizumab-IRDye800CW and quantified the ability to detect fluorescent agents administered at micro-dosing amounts. The underlying threshold analysis and biodistribution study was part of a clinical molecular imaging study of breast cancer using fluorescence-labeled bevacizumab in 20 patients with breast cancer of whom 19 patients were eligible for analysis. Tracer application was concluded to be safe and details are described in Lamberts and colleagues (1).

Patients and Methods

Clinical study

We administered bevacizumab conjugated to the near-infrared (NIR) fluorescent dye IRDy800CW (i.e., bevacizumab-IRDye800CW) to breast cancer patients. Drug labeling was achieved at the University Medical Center Groningen under therein established Good Manufacturing Practices (GMP; ref. 2). Bevacizumab-IRDye800CW is already considered in clinical trials for surgical and endoscopic guidance (ClinicalTrials.gov numbers: NCT01508572, NCT01972373, and NCT02113202). Nineteen patients diagnosed with breast cancer at mean age 64.6 years (10.26 years SD) have been included in this analysis. Tumor sizes, evaluated at pathology, averaged at 20.1 mm (7.9 mm SD). Consistent with micro-dosing regulations, as described in the FDA guidelines "Guidance for Industry, Investigators, and Reviewers Exploratory IND Studies," 4.5 mg of labeled bevacizumab (<30 nmol of labeled antibody) were administered to patients 3 days before surgery (see Supplementary Section for details).

Development of fSTREAM

To achieve the study objectives, we developed comprehensive analysis of fluorescent human tissue specimen at multiple scales (Fig. 1). Termed *f*STREAM, the analysis coregisters (i) color images, (ii) fluorescence images, (iii) hematoxylin and eosin (H&E) mosaic–stained microscopy slices, and (iv) the pathologists demarcation border obtained from an excised cancer specimen, onto a common geometrical frame. Subsequently, statistical processing of the 4-modal hybrid image was carried-out to guide threshold selection by studying bevacizumab-IRDye800CW distribution in human breast cancer. The study obtained multiscale measurements from tissue specimen at the macroscopic, mesoscopic, and microscopic scales, that is:

Macroscopic tumor imaging, based on a real-time color and fluorescence composite EagleRay-V3 camera, custom-developed at the Helmholtz Zentrum München and Technical University of Munich (see Supplementary Material; refs. 3, 4) and approved for clinical use by the Institutional Review Board of the University Medical Center Groningen. EagleRay-V3 video and images were simultaneously acquired during surgery (Fig. 1B) at a field of view (FOV) of approximately 15 cm × 15 cm and resolution of 150 μm. Immediately after the excision, the surgical specimen was placed on a table and imaged (Fig. 1C) with the same EagleRay-V3 parameters.

Mesoscopic EagleRay-V3 color and fluorescence imaging was then performed on freshly excised 3-mm thick lamellae (Fig. 1E) using mesoscopic parameters, that is, 2 cm × 2 cm FOV and 20 micrometer resolution. Shortly after, the lamellae were fixed in paraffin. Paraffin blocks were also imaged with mesoscopic imaging settings (Fig. 1F) using the EagleRay-V3 camera or flat-bed scanning (Odyssey, LI-COR Biosciences). Details are outlined in the Supplementary Material "Fluorescence validation, H&E & VEGF-A Staining."

Microscopic mosaicking imaging was then performed on consecutive 4-μm thick histologic slices obtained from the paraffin blocks, covering the same field of view as in mesoscopic imaging (Fig. 1G). The histology slices were stained with H&E and tumor demarcation was performed by experienced pathologists. All pathologists were blinded to the fluorescence signals during the classification process. Interleaved histology slices not processed by H&E were stained for VEGF-A expression using the polyclonal IgG VEGF A-20 Antibody (sc-152, Santa Cruz Biotechnology) and imaged with conventional microscopy; (For details see Supplementary Material section "Fluorescence validation, H&E & VEGF-A Staining").

Color and fluorescence images, obtained from paraffin blocks, were registered onto the corresponding H&E mosaic image obtained from the same field of view. Then the pathologists' tumor segmentation on the H&E image was recorded and registered on the color, fluorescence and H&E images. Image registration was based on affine transformations utilizing six or more anatomic landmarks. The 4-modality coregistration was an essential *f*STREAM step to streamline the spatial and intensity correlations between malignant tissue area and fluorescence signals.

Identification of a global threshold

The work herein sought to develop a method that could derive an objective, quantitative global threshold for optimal cancer delineation. The use of a normalized objective global threshold is critical for the clinical application of fluorescence imaging, that is, at conditions where real-time guidance is required. The following analysis was applied to the bevacizumab-IRDye800CW breast cancer study treated herein. Nevertheless, the proposed methodology is generalizable to any fluorescence imaging study.

The first step in deriving a normalized global threshold was image normalization, so that threshold application relates to comparable images independently of gains (intensity of illumination, camera amplification), background noise (ambient light, read noise etc.), and tissue variations or amount of agent administered and patient body weight. We therefore assumed the normalized fluorescence image S_i, that is,

$$S_{ij}(\alpha,\ \beta,\ \gamma) = \frac{F_{ij}}{\alpha * mean(F_i) + \ \beta * thres(F_i)} + \ \gamma, \qquad (A)$$

whereby F_{ij} is the fluorescence intensity value of the j-th pixel of the *i*-th image of the original (raw) fluorescence image, assuming a number of fluorescence images $i = 1...N$ obtained from different patients (e.g., Figs. 2E or 3B). The parameters α, β modulate the normalization of image F_i by its mean value $mean(F_i)$ and a threshold value $thres(F_i)$; the latter indicating the value that maximizes the inter-class variance for the *i*-th image and was determined by the Otsu's method (5) for each F_i image. The parameter γ adjusts the image offset, representative of a background constant value due to bias values typically present in CCD camera images. To derive a global threshold, we determined the values $[\alpha\ \beta\ \gamma]$ by minimizing the cost function $C([\alpha,\ \beta,\ \gamma])$ that is:

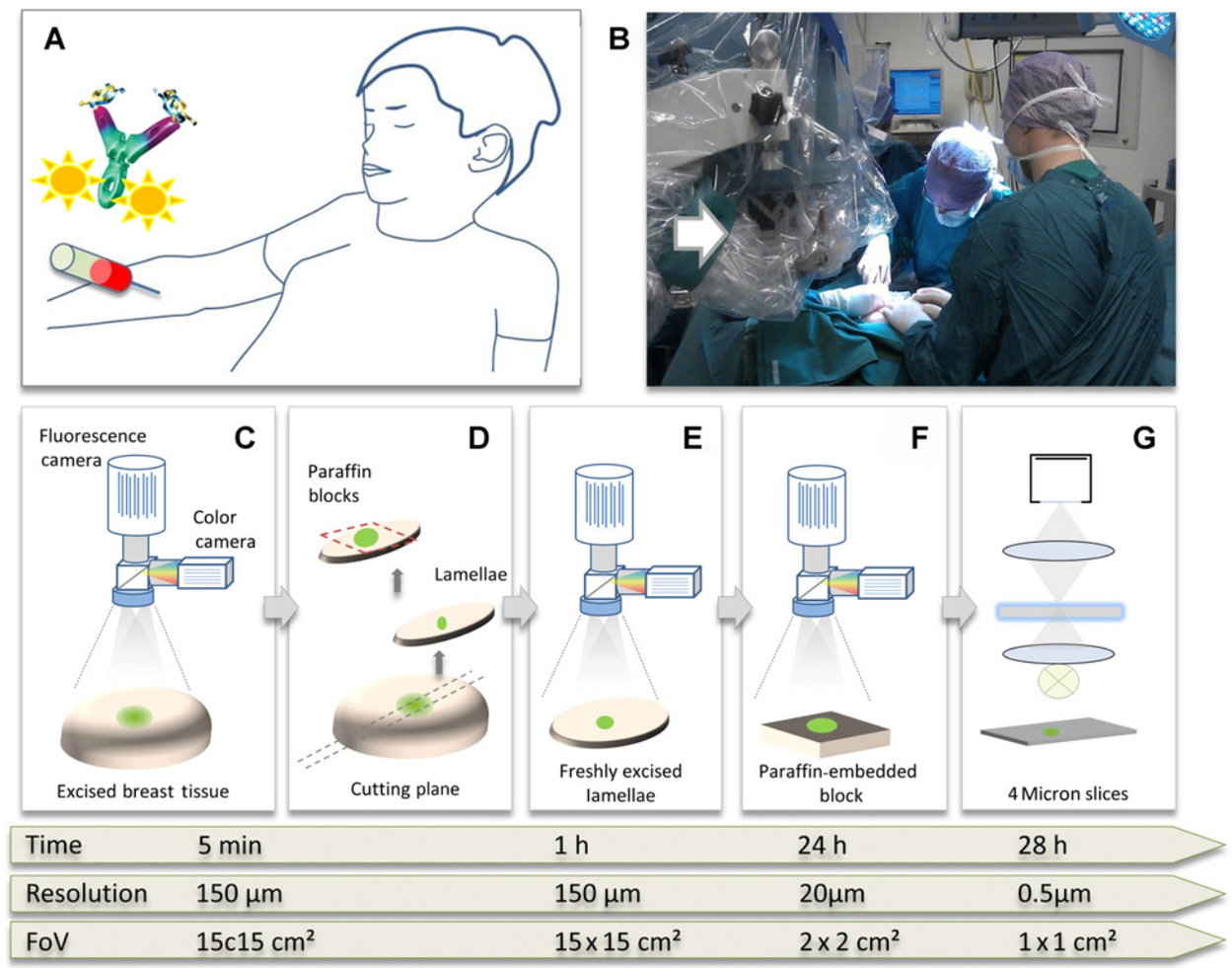

Figure 1.

*f*STREAM imaging pipeline from *in situ*/*in vivo* macroscopy to *ex vivo* mesoscopy and microscopy. **A,** Bevacizumab-IRDye800CW was systemically administered to breast cancer patients 72 hours before surgery. **B** and **C,** Macroscopic real-time fluorescence and color epi-illumination images were acquired during surgery (**B**) and from excised breast tissue approximately 5 minutes post-surgery (**C**): (field of view of 10 cm × 10 cm). **D,** Excised tissue was subsequently cut to 3 mm lamellae and casted in 2 cm × 3 cm blocks embedded into paraffin. **E,** Mesoscopic imaging of fresh excised lamellae was performed immediately after step **D**. **F,** Paraffin-embedded tissue blocks were then imaged with a 2 cm × 2 cm field of view and 20 micrometer resolution. **G,** Mosaicking H&E microscopic imaging was then performed on 4-µm slices obtained from the paraffin blocks imaged in step **F**. Histological imaging was also performed on slices stained for VEGF.

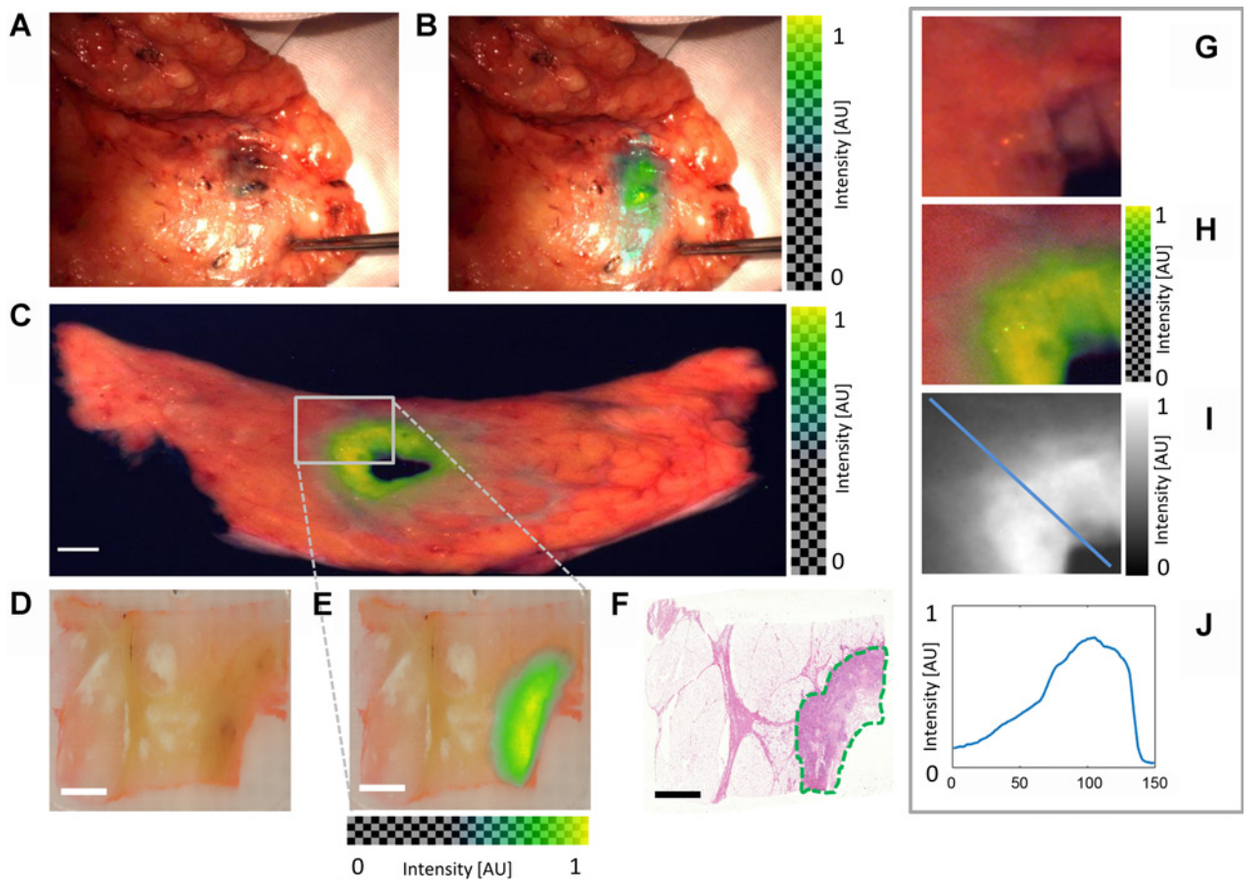

Figure 2.

Spatial patterns of bevacizumab-IRDye800CW distribution in an invasive ductal carcinoma. **A** and **B,** Color (**A**) and hybrid color (**B**) and fluorescence image of deep-seated breast tumor during a mastectomy *in situ*. The fluorescence signal is overlaid in green pseudo-color onto the color reflectance image. **C,** Fresh lamella of 3-mm thickness obtained from breast tissue specimen containing a tumor. The tumor is marked in this view with a green pseudo-color. Note that this image is taken directly from a cut through the tumor and the signal exhibits much less diffusion than in **B**. Necrosis has developed in the core of the tumor. Scale bar, 10 mm. **D,** Color image of the paraffin-embedded tissue sample obtained from an area delineated on **C** by a white rectangle. Scale bar, 5 mm. **E,** Fluorescence image of the same area overlaid in green pseudo-color on the color image shown in **D**. **F,** H&E staining of 4-μm thick paraffin slice corresponding to the field of view in **D**. The green dotted line marks the tumor border according to histopathology. Scale bar in **D–F**, 5 mm. **G–I,** Magnifications of color (**G**), pseudo-color overlay (**H**), and raw fluorescence images obtained from the region outlined by the rectangle in subfigure **C** (**I**). **J,** Fluorescence intensity profile along the blue line shown in **I**. High fluorescence photon diffusion is visible on the images, leading to an uncertain tumor border delineation.

$$C(\alpha,\ \beta,\ \gamma) = \ (1 - \ AUC(S([\alpha,\ \beta,\ \gamma]),\ G\ )) \qquad \text{(B)}$$

where G is a binary image, indicating the areas of malignant versus nonmalignant tissue on the image S, as obtained by the congruent H&E pathology segmentation, and AUC is the area under the receiver-operator-characteristics (ROC) curve (the normalized Mann–Whitney-Wilcoxon test). The optimal $[\alpha\ \beta\ \gamma]$ parameters used in image normalization (Eq. A) were estimated by an unconstrained nonlinear optimization.

ROC analysis

ROC analysis was performed on data from all specimen measured and processed by Eq. A, using the image normalization parameter set $[\alpha\ \beta\ \gamma]$ obtained by Eq. B. To inspect whether the use of a global threshold did not produce any outliers in the data set examined, we solved (minimized) Eq. B 21 times. Each time, the minimization used 21 samples to derive the global threshold and excluded a different sample from the training set.

Homogeneity of bevacizumab-IRDye800CW distribution

The study further examined the patterns of bevacizumab-IRDye800CW in human breast cancer. To quantify the spatial pattern observed, we calculated entropy values for areas of $(0.5\ \text{mm})^2$ on the raw fluorescence tumor images obtained from the paraffin blocks. The bevacizumab-IRDye800CW distribution pattern at a higher resolution was also interrogated by analyzing images acquired from 4-μm slices obtained from each of the 3-mm thick lamellas used for the entropy analysis.

Results

Pattern of bevacizumab-IRDye800CW distribution in breast cancer

Fluorescence images obtained *in situ* or post-surgery from excised specimen (Fig. 2A and B) exhibited patterns of diffusive appearance. In breast cancer surgery a positive margin is defined as "ink-on-tumor" according to the 2014 SSO/ASTRO guidelines

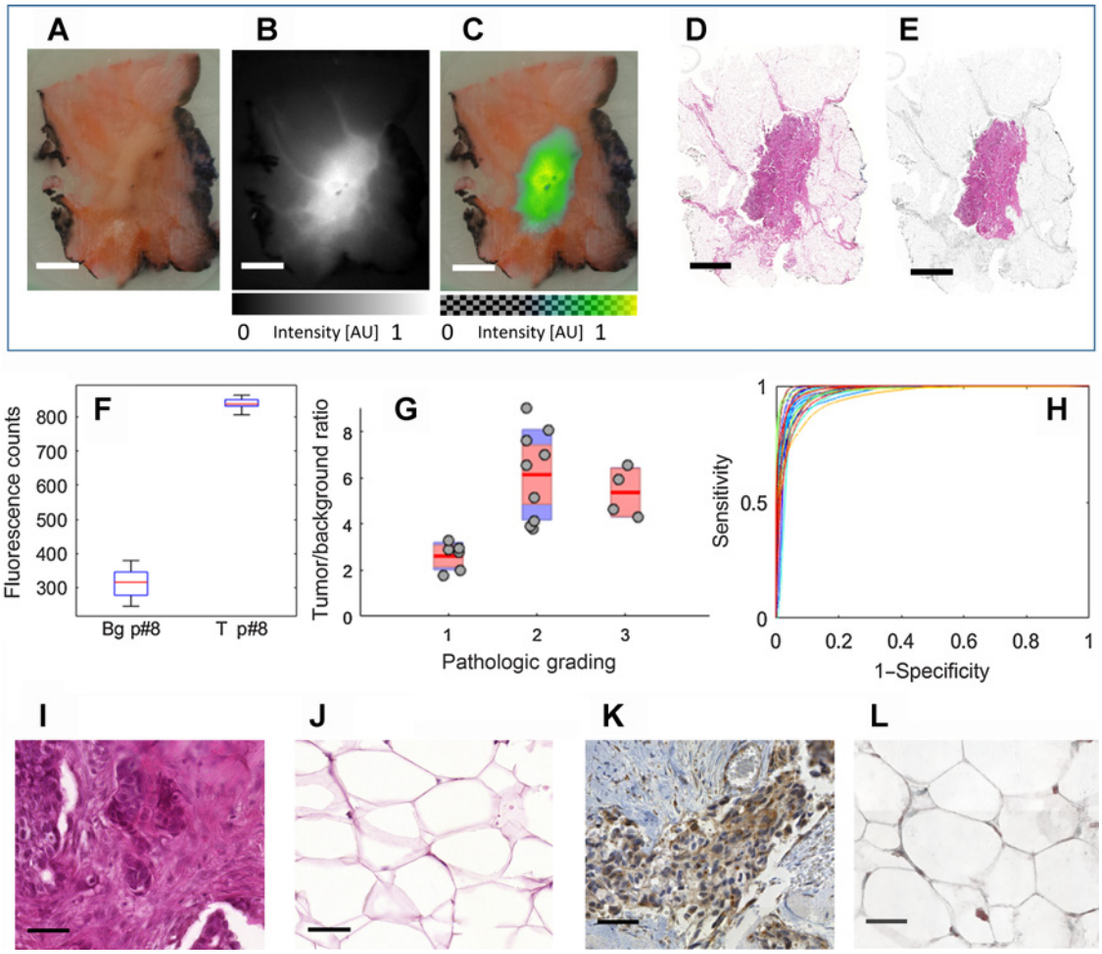

Figure 3.

Image coregistration, target-to-background analysis, and spatial correlation of fluorescence and histological data. Images in **A–E** were registered to each other by affine transformation based on (>6) morphological features. **A,** Color image of the examined paraffin sample from a patient. **B,** Fluorescence image of the same view. **C,** Alpha-blending overlay of pseudo-colored fluorescence signal and color reflectance image. **D,** Corresponding H&E staining of the same speciment. **E,** Tumor location according to pathology outline. Gray, background tissue. Purple, malignant areas. Scale bar in **A–E**, 5 mm. **F,** Box plot of signal distribution of background region (left box) vs. tumor region (right box) for the sample in **A–E**. **G,** Scatter plot of tumor-to-background ratios versus pathological grading for all patient samples; the red lines show the mean for each pathological grading group. The 95% confidence interval is marked in pink, whereas 1 SD is colored in blue. **H,** ROC for all patient samples revealing the performance of a pure value-driven binary classification in means of sensitivity vs. specificity. **I** and **J,** Magnified view of H&E-stained tumor region and noncancerous tissue, respectively. **K** and **L,** Corresponding VEGF-A20 staining of tumor region (**K**) and corresponding VEGF-A20 staining of nontumor tissue region (**L**). The VEGF-expression is stained in brown; hematoxylin performs cell counterstaining for reference. Scale bar in **I–L**, 50 μm.

(6); however, a margin of several millimeters to centimeters is allowed around the tumor to ensure complete tumor resection. Therefore, diffusive appearance of fluorescence signals indicated a complete (R_0) resection, that is, no ink on tumor. Signals from tumors as deep as at least 1 cm could be nevertheless detected (Fig. 2B).

Mesoscopic imaging of lamellae (Fig. 2C) offered first insights into the distribution parameters of the fluorescent bevacizumab. We observed an apparent, previously undisclosed homogenous distribution of bevacizumab-IRDye800CW throughout the tumor area. The images were obtained according to the step in Fig. 1F and demonstrate that sufficient fluorescence signal could be collected even after paraffin preservation. Occasionally, the processing of human tissue into lamellae would tear tissue in areas of low structural integrity, typically associated with necrotic areas in the tumor center, giving an appearance of openings in the middle of the tumor. Figure 2D and E show images from a paraffin embedded specimen from the rectangular area marked on Fig. 2C. These findings suggest that bevacizumab-IRDye800CW distributed in a diffusive manner throughout the tumor mass, apparently without strong influence by tumor interstitial fluid pressure or irregular perfusion (See also Figs. 3 and 4). The fluorescence images of the lamellae contain light scattering effects due to the sample thickness of 3 mm; therefore, the images in Fig. 2 are diffusive in nature. This is evidenced by inspecting fluorescence intensity profiles (Fig. 2J). Even though the borderline between tumor and healthy tissue on histologic slices is marked by pathologists as a sharp line (Fig. 2F), the fluorescence signals, as

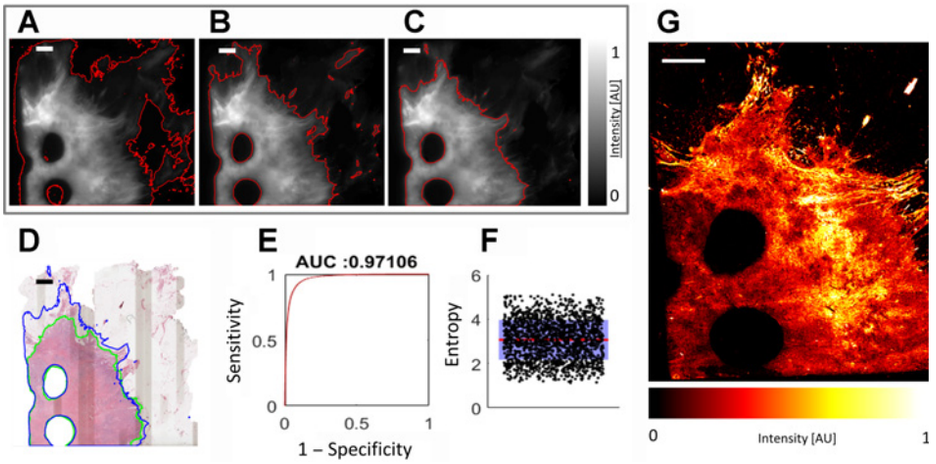

Figure 4.

Influence of threshold on segmentation. **A–C,** Fluorescence images of paraffin-embedded tissue block obtained from breast cancer stained *in vivo* with bevacizumab-IRDye800CW. The region of interest selected for different threshold levels is marked by the red line. Scale bar, 2 mm. **D,** H&E-stained slice with the gold standard segmentation by a pathologist in green and the calculated segmentation based on the fluorescence image in blue for the threshold used in **C**. **E,** ROC for all paraffin blocks when using the proposed global threshold achieving an AUC of 0.97. **F,** Distribution of the entropy values on a (0.5 mm)^2 neighborhood of all segmented tumor regions of paraffin block fluorescence images. Black dots, single entropy values. Red line, the mean value. The 95% confidence interval is marked in pink, whereas 1 SD is colored in blue. The data are jittered and subsampled for visualization. The low entropy values illustrate the high homogeneity in this paraffin block image. **G,** Fluorescence image of 4-μm thick slice corresponding to **A–C** obtained from breast cancer stained *in vivo* with bevacizumab-IRDye800CW. Scale bar, 2 mm.

expected, do not exhibit sharp borders but a diffuse appearance with no distinct definition of the tumor margin (Fig. 2I and J).

Relation of bevacizumab-IRDye800CW distribution and breast cancer

A next step was to quantitatively relate bevacizumab-IRDye800CW distribution to malignant tissue. Results from patient #8 are shown on Fig. 3A–E for demonstration purposes. Color and fluorescence images (Fig. 3A and B) from the paraffin blocks were registered onto the corresponding H&E mosaic image (Fig. 3D) and the pathologists' tumor segmentation (Fig. 3E), based on affine transformations (see Materials and Methods). Raw fluorescence counts from the tumor and background tissue for patient #8 are shown on Fig. 3F, indicating a target (tumor)-to-background ratio of approximately 2.5.

The tumor-to-background ratio (TBR) for the entire sample analyzed was related to the pathologic Bloom–Richardson–Elston (BRE) tumor grade (Fig. 3G). The BRE is a breast cancer classification metric that indicates cancer aggressiveness and combines measurements of the severity of tubule formation, nuclear pleomorphism and mitotic count per area in the tumor sample analyzed. We observed that tumors of pathologic grade score 1 exhibited less fluorescence uptake compared to tumors of grade 2 and 3. Overall, the TBR values ranged from 1.8 to 9. Fluorescence signals from the paraffin sections of all patients were spatially correlated to the underlying cancer area identified on the coregistered H&E slices. A ROC curve was drawn for each patient sample, assuming different thresholds (Fig. 3H).

Histologic confirmation was corroborated by immunohistochemistry staining for VEGF-A expression, performed on interleaved paraffin sections of 4-μm thickness (Fig. 3I–F). Elevated VEGF-A expression (Fig. 3K) was shown for the tumor area but not for surrounding nonmalignant tissue (Fig. 3L).

Application of a global threshold

Figure 3H depicts the ROC curve for each patient and presents the sensitivity and specificity by which fluorescence intensity patterns demarcate the tumor area, as confirmed by H&E analysis. However, a critical parameter in interventional fluorescence imaging relates to setting an intensity threshold on the fluorescence image to differentiate cancer from healthy tissue, in the absence of an H&E analysis. Today, thresholds are empirically assigned on the basis of image appearance and may inaccurately estimate the tumor extent and surrounding tissue (see Fig. 4A–D).

The derivation of an objective normalized global threshold (see Materials and Methods) determined the optimal $[\alpha\ \beta\ \gamma]$ parameters (see Eq. A and B), which were estimated to be [0.9240, 1.3103, and 0.0040] for the set of 22 paraffin block samples from the 19 patients examined (double paraffin samples were available in pathology from 3 patients with large tumors). The ROC analysis considered all specimen images processed by Eq. A using image normalization based on the optimal parameter set $[\alpha\ \beta\ \gamma]$. The resulting ROC curve (Fig. 4E) achieved an AUC value of 0.97 for all 22 samples examined. We note that skin regions exhibited elevated fluorescence but were not included in the analysis (see Fig. 1 in Supplementary Material for details). To confirm the generality of the global threshold, we computed the AUC variation between an excluded sample and the remaining set of samples (see Materials and Methods). The AUC variation was $\pm$ 0.00389%, indicating that the application of the global threshold did not produce any outliers in any of the data sets examined.

Homogeneity of bevacizumab-IRDye800CW distribution

Figures 2 and 3 showcase a rather homogeneous distribution of bevacizumab-IRDye800CW throughout tumors. Entropy

calculations (see Materials and Methods) quantified the spatial pattern observed on the raw fluorescence tumor images from paraffin blocks (Fig. 4F). The mean entropy value for all patient samples was 3.06 with an SD of ± 0.81 for a $(0.5\ \text{mm})^2$ neighborhood; a finding that confirms a homogeneous pattern of labeled drug distribution in all patient samples examined.

Entropy analysis of 4-μm slices obtained from each of the 3-mm thick lamellas employed was also considered for higher-resolution bevacizumab-IRDye800CW observations, because images from the 4-μm slices are virtually scatter-free. The corresponding voxels represented on Fig. 4G are of lower total volume compared with the voxels observed in Fig. 4A–C. The entropy value for a $(0.5\ \text{mm})^2$ area within tumors was 6.4374 ± 0.81006. As expected, the entropy increases when observing higher resolution images, but nevertheless showcases also a homogeneous distribution, which remains overtly constant from patient to patient. We further observed that even in high-resolution view, the fluorescence pattern generally matched the H&E outlined tumor border, although it marginally overestimated the tumor border (Fig. 4D). A comparison of magnified views from 4-μm thick versus paraffin block images is shown in Supplementary Fig. S2.

Discussion

fSTREAM was proposed as methodology for standardized analysis of fluorescence images obtained from tissues after the administration of fluorescent agents *in vivo*. The method was applied to analyze breast cancer specimen labeled with bevacizumab-IRDye800CW, obtained from a phase I clinical trial and guide the selection of a normalized objective global threshold, that is, a single normalized value derived to optimally separate malignant tissue from surrounding healthy tissue in the entire study. It was found that derivation of an objective global threshold required appropriate image normalization, performed by Eq. A, so that the intensity seen on different images is calibrated to the same reference (standard). The derivation of a normalized threshold further ensures a metric that is independent of the exact amount of agent administered, patient body weight or absolute fluorescence intensity values, since it classifies tissues based on relative intensities and in relation to the overall image statistics (Eq. A). It is nevertheless expected that the *fSTREAM* analysis is applied on a per-study basis, because the threshold value will depend on the particular type of tracer used and possibly the tissue type targeted. Therefore, data collected during a phase I study conducted for a new tracer could be analyzed to derive a threshold for use in subsequent exploratory phases or during interventional procedures. Naturally, additional data obtained from phase II/III studies may be retrospectively used to further optimize the threshold.

The proposed methodology does not involve modification of the specimen analyzed, because it uses samples in paraffin blocks and conventional histology slices; therefore, it can be seamlessly incorporated into the routine histopathological analysis workflow.

Today, fluorescence images using targeted agents are evaluated on the basis of the assumption that stronger signal implies malignancy. Correspondingly, it is typical to render the stronger fluorescence intensities of a fluorescence image in pseudocolor, together with a color image as shown in Fig. 3C. This rendering operation implies the application of a threshold on the fluorescence image depicted. However, due to the diffusive nature of fluorescence photons collected from tissues, the exact relation of fluorescence intensity/threshold and malignancy is not known; thresholds are typically user-dependent, empirical in nature, and therefore prone to errors. Observations of Fig. 2G–J showcase that there exists no clear border for cancer differentiation when performing fluorescence imaging of tissues, due to photon diffusion effects that reduce the resolution of the fluorescence image. Therefore, the selection of an objective global threshold is critical for the clinical application of fluorescence imaging, especially in association of guiding cancer resection and observing for tumor borders.

A central *fSTREAM* target was the rigorous relation of fluorescence signals to cancer. Therefore, an important parameter in the analysis proposed was the registration of the tumor demarcation by pathologists on H&E slices and corresponding fluorescence images. Affine transforms allowed a per-pixel analysis of fluorescence intensities and the underlying presence of malignant versus nonmalignant cells. Then automatic statistical analysis on a pixel-to-pixel basis enabled accurate and statistically significant correlation between pathological classification and tumor-to-background fluorescence intensity ratios.

The analysis intrinsically also observed the unknown distribution pattern of bevacizumab-IRDye800CW in human breast cancer, demonstrating broad presence in the entire tumor mass. We confirmed that the labeled drug can be detected at micro-dosing amounts (30 nmol/patient) and can be assessed at macroscopic and mesoscopic scales. ROC analysis calculated a sensitivity of 98% and a specificity of 79% when using fluorescence signals to outline the tumor mass. Breast cancer surgery is reported to yield up to approximately 30% positive tumor margins, directing secondary procedures (7). Hence, the findings herein preliminary showcased that bevacizumab-IRDye800CW may be valuable for intraoperative breast cancer margin detection, a hypothesis that is currently investigated in a follow-up phase II clinical study (ClinicalTrials.gov Identifier: NCT02583568). It was suggested that fluorescent bevacizumab selectively labels cancer in xenograft animals (8) and can be used for imaging studies, even if it only targets soluble VEGF-A (9, 10). Staining for VEGF-A expression revealed elevated VEGF levels in all tumors studied herein. Nevertheless, it is likely that the homogeneous distribution pattern observed is influenced by enhanced permeability and retention effects.

We also observed bevacizumab-IRDye800CW presence in areas not rich in VEGF expression including the skin and breast ducts. The sensitivity and specificity data reported were calculated only for the area (volume) around the tumor, as defined by the surgical specimen, not for the entire breast tissue, and it therefore relates more closely to intraoperative observations and not breast cancer diagnosis in the radiological sense.

Labeled drugs have been considered for imaging studies due to their general availability and expectation that the biodistribution and targeting profile of the labeled molecule will not significantly vary over the unlabeled counterpart, especially when labeling antibodies (11–13). Radionuclide-labeled drugs are often assessed with positron emission tomography to quantitatively determine the dose of an administered therapeutic molecule delivered into different organs, whereas other, nontherapeutic molecules are considered for diagnostic and staging purposes (14, 15). Examples include imaging of anti-folate agents (16) or monoclonal antibodies (8, 10). However, while nuclear imaging

studies enable full-body scans, the low spatial resolution achieved only allows assessment of the macro-distribution at volume sampling of approximately 0.1–1 cm^3 (17). *fSTREAM* comes with the potential to study the labeled molecule at higher-resolution, within the tumor microenvironment and better understand long-term biodistribution within the cancer lesion, albeit it can only be applied as an invasive technique within surgery and endoscopy.

Overall, fSTREAM can be employed for the systematic analysis of new classes of fluorescent agents considered for human use and broader disease targets (8, 11). Moreover, it can be considered as an alternative method to elucidate human cancer biology by observing personalized readings of cancer pathophysiology on excised specimen following fluorescence-guided procedures using targeted agents. The high sensitivity of the method allows micro-dosing observations, possibly relaxing regulatory parameters. Such application could capitalize on the emerging clinical practice of using fluorescent agents for diagnostic purposes (18–22).

Disclosure of Potential Conflicts of Interest

J.S. de Jong is a consultant/advisory board member for SurgVision. W.B. Nagengast reports receiving a commercial research grant from SurgVision unrestricted research grant. G.M. van Dam reports receiving a commercial research grant and is a consultant/advisory board member for SurgVision BV. V. Ntziachristos has ownership interest (including patents) in Equity holder (SurgVision BV) and is a consultant/advisory board member for scientific advisory board. No potential conflicts of interest were disclosed by the other authors.

Authors' Contributions

Conception and design: L.E. Lamberts, A.L.L. Adams, C.P. Schröder, S.G. Elias, A.J. Witkamp, W.P.T.M. Mali, E. Van der Wall, P.J. van Diest, E.G.E. de Vries, G.M. van Dam, V. Ntziachristos

Development of methodology: M. Koch, J.S. de Jong, J. Glatz, P. Symvoulidis, A.L.L. Adams, A.G.T. Terwisscha van Scheltinga, M.N. Lub-de Hooge, C.P. Schröder, S. Oliveira, P.J. van Diest, E.G.E. de Vries, G.M. van Dam, V. Ntziachristos

Acquisition of data (provided animals, acquired and managed patients, provided facilities, etc.): M. Koch, J.S. de Jong, J. Glatz, P. Symvoulidis, L.E. Lamberts, A.L.L. Adams, M.E.G. Kranendonk, M. Aichler, L. Jansen, J. de Vries, M.N. Lub-de Hooge, C.P. Schröder, E. de Boer, B. van der Vegt, W.B. Nagengast, S. Oliveira, A.J. Witkamp, W.P.T.M. Mali, P.B. Garcia-Allende, P.J. van Diest, E.G.E. de Vries, A. Walch, G.M. van Dam

Analysis and interpretation of data (e.g., statistical analysis, biostatistics, computational analysis): M. Koch, J.S. de Jong, J. Glatz, P. Symvoulidis, L.E. Lamberts, M.E.G. Kranendonk, M. Aichler, S. Oliveira, E. Van der Wall, P.J. van Diest, A. Walch, G.M. van Dam, V. Ntziachristos

Writing, review, and/or revision of the manuscript: M. Koch, J.S. de Jong, J. Glatz, P. Symvoulidis, L.E. Lamberts, A.L.L. Adams, A.G.T. Terwisscha van Scheltinga, M. Aichler, J. de Vries, M.N. Lub-de Hooge, C.P. Schröder, A. Jorritsma-Smit, B. van der Vegt, W.B. Nagengast, S.G. Elias, A.J. Witkamp, E. Van der Wall, P.J. van Diest, E.G.E. de Vries, G.M. van Dam, V. Ntziachristos

Administrative, technical, or material support (i.e., reporting or organizing data, constructing databases): M. Koch, P. Symvoulidis, M.E.G. Kranendonk, A.G.T. Terwisscha van Scheltinga, M.N. Lub-de Hooge, A. Jorritsma-Smit, M.D. Linssen, E. de Boer, B. van der Vegt, P.B. Garcia-Allende, G.M. van Dam

Study supervision: G.M. van Dam, V. Ntziachristos

Grant Support

V. Ntziachristos received funding from the Leibniz Prize 2013 (NT 3/10-1). E.G.E. de Vries, P.J. van Diest, and W.P.T.M. Mali received funding from the Center for Translational Molecular Medicine, project MAMMOTH (grant 03O-201), E.G.E. de Vries has received funding from the ERC Advanced grant OnQView and S.G. Elias from the Dutch Cancer Society KWF by a research fellowship.

The costs of publication of this article were defrayed in part by the payment of page charges. This article must therefore be hereby marked *advertisement* in accordance with 18 U.S.C. Section 1734 solely to indicate this fact.

Received July 21, 2016; revised October 6, 2016; accepted October 24, 2016; published OnlineFirst November 22, 2016.

References

1. Lamberts LE, Koch M, de Jong JS, Adams A, Glatz J, Tranendonk MEG, et al. Tumor-specific uptake of fluorescent bevacizumab-IRDye800CW microdosing in patients with primary breast cancer: a phase I feasibility study. Clin Cancer Res 2016.
2. ter Weele EJ, van Scheltinga AGT, Linssen MD, Nagengast WB, Lindner I, Jorritsma-Smit A, et al. Development, preclinical safety, formulation, and stability of clinical grade bevacizumab-800CW, a new near infrared fluorescent imaging agent for first in human use. Eur J Pharm Biopharm 2016;104:226–34.
3. Themelis G, Yoo JS, Soh K-S, Schulz R, Ntziachristos V. Real-time intraoperative fluorescence imaging system using light-absorption correction. J Biomed Opt 2009;14:064012.
4. Glatz J, Varga J, Garcia-Allende PB, Koch M, Greten FR, Ntziachristos V. Concurrent video-rate color and near-infrared fluorescence laparoscopy. J Biomed Opt 2013;18:101302.
5. Otsu N. A threshold selection method from gray-level histograms. Automatica 1975;11:23–7.
6. Moran MS, Schnitt SJ, Giuliano AE, Harris JR, Khan SA, Horton J, et al. SSO-ASTRO consensus guideline on margins for breast-conserving surgery with whole breast irradiation in stage I and II invasive breast cancer. Int J Radiat Oncol Biol Phys 2014;88:553.
7. Houssami N, Macaskill P, Marinovich ML, Morrow M. The association of surgical margins and local recurrence in women with early-stage invasive breast cancer treated with breast-conserving therapy: a meta-analysis. Ann Surg Oncol 2014;21:717–30.
8. Nagengast WB, de Vries EG, Hospers GA, Mulder NH, de Jong JR, Hollema H, et al. *In vivo* VEGF imaging with radiolabeled bevacizumab in a human ovarian tumor xenograft. J Nucl Med 2007;48:1313–9.
9. Nayak TK, Garmestani K, Baidoo KE, Milenic DE, Brechbiel MW. PET imaging of tumor angiogenesis in mice with VEGF-A–targeted 86Y-CHX-A″-DTPA-bevacizumab. Int J Cancer 2011;128:920–6.
10. Nagengast WB, Lub-de Hooge MN, Oosting SF, den Dunnen WF, Warnders F-J, Brouwers AH, et al. VEGF-PET imaging is a noninvasive biomarker showing differential changes in the tumor during sunitinib treatment. Cancer Res 2011;71:143–53.
11. Scheuer W, van Dam GM, Dobosz M, Schwaiger M, Ntziachristos V. Drug-based optical agents: infiltrating clinics at lower risk. Sci Transl Med 2012;4:134ps11.
12. van Oosten M, Schäfer T, Gazendam JA, Ohlsen K, Tsompanidou E, de Goffau MC, et al. Real-time *in vivo* imaging of invasive- and biomaterial-associated bacterial infections using fluorescently labelled vancomycin. Nat Commun 2013;4:2584.
13. Rosenthal EL, Warram JM, de Boer E, Chung TK, Korb ML, Brandwein-Gensler M, et al. Safety and tumor-specificity of cetuximab-IRDye800 for surgical navigation in head and neck cancer. Clin Cancer Res 2015;21:3658–66.
14. Van de Wiele C, Lahorte C, Oyen W, Boerman O, Goethals I, Slegers G, et al. Nuclear medicine imaging to predict response to radiotherapy: a review. Int J Radiat Oncol Biol Phys 2003;55:5–15.
15. Heusner T-A, Kuemmel S, Koeninger A, Hamami ME, Hahn S, Quinsten A, et al. Diagnostic value of diffusion-weighted magnetic resonance imaging (DWI) compared to FDG PET/CT for whole-body breast cancer staging. Eur J Nucl Med Mol Imaging 2010;37:1077–86.
16. Kamen BA, Smith AK. A review of folate receptor alpha cycling and 5-methyltetrahydrofolate accumulation with an emphasis on cell models in vitro. Adv Drug Deliv Rev 2004;56:1085–97.

17. Moses WW. Fundamental limits of spatial resolution in PET. Nucl Instrum Methods Phys Res A 2011;648:S236–40.
18. Stanga PE, Lim JI, Hamilton P. Indocyanine green angiography in chorioretinal diseases: indications and interpretation: an evidence-based update. Ophthalmology 2003;110:15–21.
19. Schaafsma BE, Mieog JSD, Hutteman M, Van der Vorst JR, Kuppen PJ, Löwik CW, et al. The clinical use of indocyanine green as a near-infrared fluorescent contrast agent for image-guided oncologic surgery. J Surg Oncol 2011;104:323–32.
20. Kennedy MD, Jallad KN, Thompson DH, Ben-Amotz D, Low PS. Optical imaging of metastatic tumors using a folate-targeted fluorescent probe. J Biomed Opt 2003;8:636–41.
21. Weber CJ, Müller S, Safley SA, Gordon KB, Amancha P, Villinger F, et al. Expression of functional folate receptors by human parathyroid cells. Surgery 2013;154:1385–93.
22. Sun JY, Shen J, Thibodeaux J, Huang G, Wang Y, Gao J, et al. *In vivo* optical imaging of folate receptor-β in head and neck squamous cell carcinoma. Laryngoscope 2014;124:E312–9.